Nonlinear Dynamics **20:** 381–399, 1999.

Modal Representation of Stress in Flexible Multibody Simulation

RICHARD SCHWERTASSEK and STEFAN V. DOMBROWSKI
Institute of Robotics and System Dynamics, German Aerospace Center (DLR), D-82234 Wessling, Germany

OSKAR WALLRAPP
Fachhochschule – University of Applied Sciences, FB 06, D-80335 München, Germany

(Received: 9 March 1999; accepted: 15 July 1999)

Abstract. An application of the floating frame of reference formulation together with the nodal approach using quasi-comparison functions as shape functions allows an efficient analysis of stress in the flexible bodies of a multibody system. This is demonstrated using two simple examples. They are chosen to demonstrate the effects of various choices of shape functions and associated body reference frames. In the floating frame of reference formulation the equations of motion are linearized assuming the deformations to be small. The quasi-comparison functions, i.e. shape functions, can be selected in ways to increase the range of validity of the linearized equations of motion. The latter goal is achieved as well by so-called substructuring techniques. Combining both of the methodologies, one obtains efficient models for flexible multibody simulation.

Keywords: Multibody simulation, flexible body modelling, modal coordinates, representation of stress.

1. Introduction

The floating frame of reference formulation for the modelling of flexible bodies in multibody systems has been reviewed in a companion paper [1]. The method is based on a separation of the flexible body motion into a reference motion and deformation. A unique definition of the two parts of the motion requires the definition of a body reference frame. This definition affects the choice of the shape functions, used in [1, equation (21)] to represent the body deformation. When modelling flexible bodies in multibody systems as finite element structures, the so-called nodal and modal approaches may be applied to describe body deformation [1, section 7]. The reduction of the number of system variables in the modal approach is highly desirable to increase computational efficiency, but the methodology results in the fundamental problem of selecting shape functions that represent body deformation and, in particular, internal forces with an appropriate accuracy. This problem appears as well when modelling beams as suggested by [1, equations (41–44)]. The selection of shape functions cannot be made in a formal way. It depends on the analyst's judgement and it is emphasized in [1, figure 8] by the circle in the flowchart for the computation of the standard body data.

The reference motion of a flexible body i in a multibody system is large in general, but its deformation as represented by the variables $\mathbf{u}^i(\mathbf{R}, t)$ and $\boldsymbol{\vartheta}^i(\mathbf{R}, t)$ (see [1, equation (21)]) remains small in many applications. In such cases the computational efficiency of a system simulation can be increased by linearizing the dynamical equations of motion, equation (26) in [1], for small deformation. The linearization procedure may require the consideration of geometric stiffening, applying the general rules given in [1, section 6].

An additional possibility to improve computational efficiency is provided by the modal approach. The resulting problem of selecting the shape functions is of particular importance for the representation of the stresses in the flexible system bodies. Often, flexible multibody system codes provide good results to describe the body deformation, whereas the representation of stresses cannot be used for system evaluation. To overcome such deficiencies, it has been proposed to determine the stresses by post-processors, using finite element codes [2]. But an acceptable representation of internal forces in the flexible system bodies can be obtained with multibody codes as well when using quasi-comparison functions [3–7]. As mentioned in [1, sections 1 and 7], a set of quasi-comparison functions may be obtained by combining eigenfunctions and static deformation modes.

A good representation of stress is obtained automatically by methods, which generalize the concepts of finite elements to multibody systems [8]. A general problem in such methods is to model large rotational motion of the elements [9]. System simulations based on the corresponding nonlinear finite element formulations often result in high computational costs [10]. To avoid them, various approximations have been proposed. An example is [11, 12], where multibody and finite element codes are coupled to obtain an iterative calculation scheme for flexible multibody analysis: the flexible bodies are assumed to be 'frozen' in their deformed configuration when a multibody code is applied to compute the system motion and the resulting inertia and constraint forces upon the bodies. Using these forces in a finite element code, the body deformation and the stresses are updated neglecting the coupling effects between rigid body motion and deformation. A method taking into account such effects has been described in [13] and literature cited there. Procedures of how to compute the stresses based on the floating frame of reference formulation have been proposed in [14, 15]. In the latter reference stress influence coefficients are introduced to increase computational efficiency. The methods are proposed for fatigue life prediction and stress-safe design. The former application is discussed in [16] as well. Among others, the computational benefits of symbolic code generation are analysed. The stresses are computed by the modal approach using beam models and applying the general data structure from [1, figure 8].

The representation of stress by quasi-comparison functions in the floating frame of reference formulation will be discussed here together with the two possibilities to reduce computational costs, i.e. the application of the modal approach and of the linearized equations assuming the deformations to be small. The discussion is based on two simple examples. The first one gives an analysis of the effects of various shape functions on the representation of deformation and in particular of internal forces. An application of the linearized equations requires the deformations to be as small as possible. In the second example it will be demonstrated that a wide range of applicability of the linearized equations may be achieved by selection of the shape functions and by subdividing the flexible bodies as proposed in [17]. A combination of the two methodologies provides efficient system equations for an analysis of flexible multibody systems.

2. Effects of Shape Functions on Representation of Deformation and Stress

2.1. Study Model

For a discussion of the choice of shape functions, the structure shown in Figure 1 is considered. It consists of a flexible beam AB, which is connected to a rigid body BC by a bracket joint, allowing no relative motion. The beam is attached at points A and D to a fixed, supporting

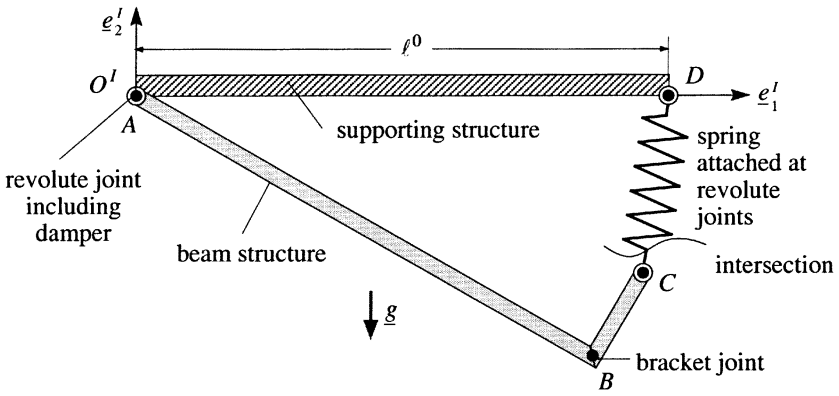

Figure 1. Rotating beam structure supported by a spring.

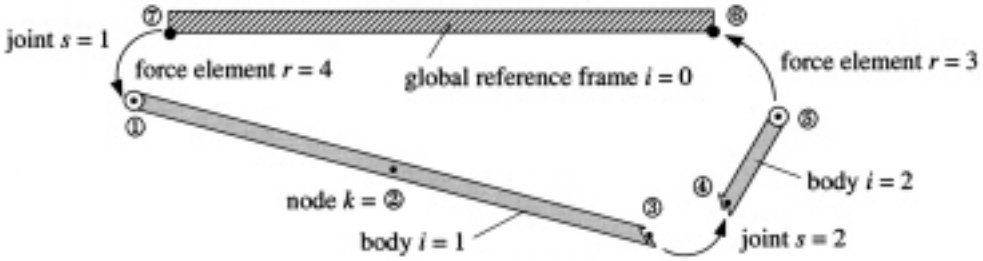

Figure 2. Multibody model of the beam structure. Node labels are encircled. General node-, joint- and force element-labels are k, s and r, respectively. The arrows at the joints and force elements show the way, in which the relative motion across those interconnections is defined.

structure. At A, there is a revolute joint together with a rotational damper. Point D is connected with C by a spring. External forces acting on the structure are the result of gravitational acceleration, defined by the vector $\underline{g}$. The notation used here is as described in [1].

The influence of shape functions is studied by analyzing the

- equilibrium configuration I, in which the structure is supported by the spring;
- motion and the equilibrium configuration II, obtained after cutting the spring at C;
- internal forces in the beam AB in the equilibrium configuration II.

The problems are solved using the multibody model shown in Figure 2. Origin and basis of an inertial frame (identical with the global reference frame $i = 0$) are shown in Figure 1. In this frame the coordinates of the gravitational acceleration are $[0, -g, 0]^T$, $g = 9.81$ m/s^2. The distance of the points A and D is $\ell^0 = 2$ m.

To represent the motion of body $i = 1$ by the variables given by [1, equation (22)], a body reference frame has to be defined. The three types of frames indicated in [1, figure 5] (the tangent-, chord- and Buckens-frame) will be compared. Figure 3 shows a chord-frame, the variables of [1, equation (22)] representing its motion and the variables $w_1^1(x,t)$ and $w_2^1(x,t)$, $x \equiv R_1$, describing the deformation of the beam (see also [1, figure 6]). The data of the beam model are: length $\ell^1 = 2$ m, height $h^1 = 0.003$ m, area of cross section $A^1 = 0.0006$ m^2, area moment of inertia of the cross section $J^1 = 4.5 \cdot 10^{-10}$ m^4, density $\rho^1 = 8400$ kg/m^2 and modulus of elasticity (Young's modulus) $\mathcal{E}^1 = 7 \cdot 10^{10}$ N/m^2.

Body 2 is rigid, and Figure 4 shows the location and orientation of its reference frame $\{O^2, \underline{\mathbf{e}}^2\}$. In this frame the data of the body are: location of center of mass $\mathbf{c}^2 = [0.2, 0, 0]^T$ m

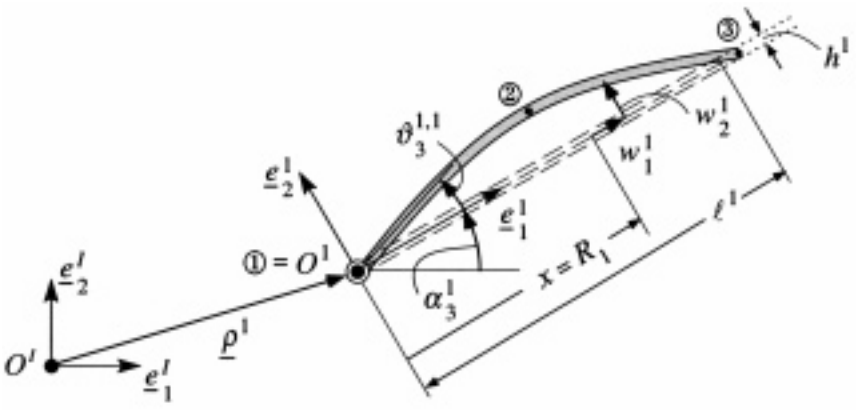

Figure 3. Notation used to represent the motion of body $i = 1$.

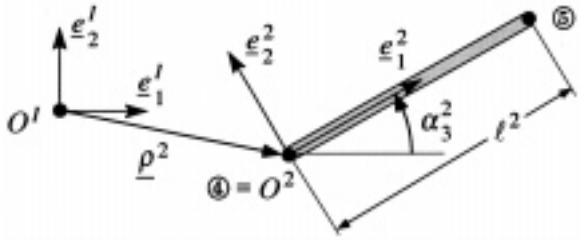

Figure 4. Notation used to represent the motion of body $i = 2$.

and moment of inertia $I^2 = 0.32 \cdot 10^{-10}$ kg m^2, given with respect to the origin O^2 of the body frame. The length of the body is $\ell^2 = 0.4$ m.

The nodes on the bodies are specified by matrices $\mathbf{R}^{k,i}$ and $\mathbf{\Gamma}^{k,i}$, introduced in [1, equations (2–4)]. For most of the nodes, $\mathbf{R}^{k,i} = \mathbf{0}$ and $\mathbf{\Gamma}^{k,i} = \mathbf{E}$. The matrices having different values are

$$\mathbf{R}^{2,1} = \begin{bmatrix} 1 \\ 0 \\ 0 \end{bmatrix}, \quad \mathbf{R}^{3,1} = \begin{bmatrix} 2 \\ 0 \\ 0 \end{bmatrix}, \quad \mathbf{R}^{5,2} = \begin{bmatrix} 0.4 \\ 0 \\ 0 \end{bmatrix},$$

$$\mathbf{R}^{6,0} = \begin{bmatrix} 2 \\ 0 \\ 0 \end{bmatrix}, \quad \mathbf{\Gamma}^{3,1} = \begin{bmatrix} 0 & 1 & 0 \\ -1 & 0 & 0 \\ 0 & 0 & 0 \end{bmatrix} \tag{1}$$

with the $\mathbf{R}^{k,i}$ given in m. Node $k = 2$ on body $i = 1$ is not required for attachment of a system element – it is used to define a point for evaluation of deformation and internal forces.

The axis of the rotational joint at A is given in the basis $\underline{\mathbf{e}}^1$ by $[0, 0, 1]^T$. The force element $r = 4$ at this joint results in a torque about $\underline{\mathbf{e}}_3^1$, depending linearly on the relative angular velocity across the interconnection – the damping factor is 40 N ms/rad. The spring, connecting the nodes $k = 5$ and $k = 6$, has an undeformed length of 0.1 m, and its stiffness is 300 N/m.

2.2. Definition of the Deformation Models

To solve the problems mentioned above, three groups of models are used to represent the deformation of body 1. They correspond to a chord-, tangent- and Buckens-frame and are

distinguished by labels C, T and B, respectively. The displacements of the beam's axis result from stretching and bending and they are represented by $n_q^1 = n_{q1} + n_{q2}$ shape functions in the form

$$w_1^1(x,t) = \sum_{i=1}^{n_{q1}} W_{1j}^1(x)\, q_j^1(t), \quad w_2^1(x,t) = \sum_{j=1}^{n_{q2}} W_{2j}^1(x)\, q_k^1(t) \quad \text{where} \quad k = n_{q1} + j. \quad (2)$$

A variety of models, all of them using the chord-frame as the body reference frame, will be considered first. In these models the deformation of body $i = 1$ is described as suggested by Equation (2), using various numbers and types of shape functions. The models are characterized by identifiers, which are combinations of C and consecutive numbers. In addition to the identifiers, the numbers $n_q^1(t)$ of variables $q_j^1(t)$, which are used to represent deformation, are given in parentheses. The models are:

C1(2): The first eigenfunctions $W_{11}^1(x)$ and $W_{21}^1(x)$ for longitudinal and lateral vibrations of a simply supported beam are selected to represent deformation.
C2(6): Same as C1, but 3 functions $W_{1j}^1(x)$ and 3 functions $W_{2j}^1(x)$.
C3(15): Same as C1, but 5 functions $W_{1j}^1(x)$ and 10 functions $W_{2j}^1(x)$.
C4(6): Same as C2, but the shape functions used here are based on eigenfunctions of a beam, which is supported by a rotational joint at $x = 0$. By consequence, a (rotational) rigid body mode appears among the eigenfunctions. It is deleted and to obtain the shape functions. The remainder of the eigenfunctions is transformed, as suggested in [18], to satisfy the chord-frame boundary conditions.
C5(2): In this case $W_{11}^1(x)$ and $W_{21}^1(x)$ are the static deformations of a simply supported beam due to a longitudinal force and to a torque at node $k = 3$, respectively.
C6(4): Combination of C1 and C5.
C7(8): Combination of C2 and C5.

The shape functions, used in these models, are shown in Figure 5 for C2, C4, C5 and C6. The functions used in C1 are a subset of C2, and in case of C3 additional, higher modes of the type shown for C2 are considered.

In the second group of models a *tangent-frame* is used as a body reference frame. Its origin coincides with the origin of the chord-frame shown in Figure 3. Using notation similar to the one introduced for the C-models, the tangent-frame models are:

T2(6): Same as C2, but eigenfunctions of a cantilever instead of a simply supported beam.
T7(8): Same as C7, but eigenfunctions and static forms of a cantilever beam, i.e. 3 vibration modes for both, longitudinal and lateral motion, and static forms due to a force and a torque at node $k = 3$.

The shape functions, used in the two T-models, are shown also in Figure 5.

Finally, a *Buckens-frame* is chosen for $\{O^1, \underline{\mathbf{e}}^1\}$. The location of O^1 and the orientation of $\underline{\mathbf{e}}^1$ satisfy the linearized equations (36) from [1]. This implies that O^1 coincides with the center of mass CM^1 of the deformed beam. In this case, eigenfunctions of the free-free beam are used, with the rigid body modes deleted. The models considered in this study are:

B2(6): Same as C2, but with eigenmodes of the free-free beam.

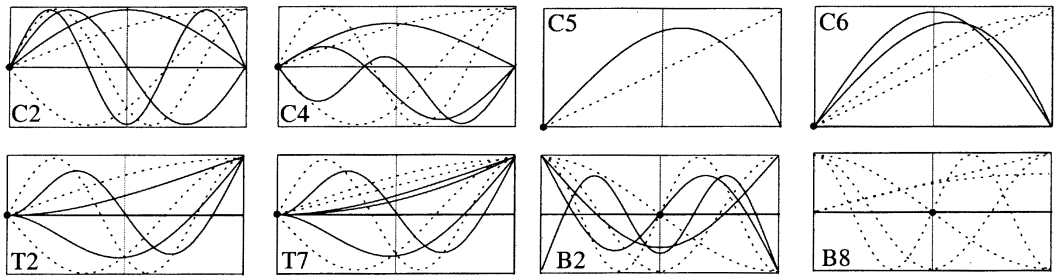

Figure 5. Mode shapes used to represent the deformation of body $i = 1$. Dotted and solid curves correspond to longitudinal and lateral motion, respectively. In all of the diagrams the horizontal axes represent values of x and in vertical direction the function values $W^1_{1j}(x)$ and $W^1_{2j}(x)$ are given.

B7(8): B2 combined with C5 – by analogy with C7.
B8(9): B7 with an additional static deformation mode of a simply supported beam, due to a linearly distributed load in the longitudinal direction.

The shape functions, used in these models, are shown in Figure 5. The diagram for B8 shows the longitudinal modes only.

The models B7(8) and B8(9) require a comment. The quasi-comparison functions, used in [1, equation (21)] to approximate the solution of the partial differential equations describing body deformation, have to be elements of a complete set of functions, they have to satisfy the geometrical boundary conditions and a linear combination of them has to be capable to satisfy the dynamical boundary conditions. In case of a Buckens-frame the body deformation is described by partial differential equations satisfying the constraints ${}_O\mathbf{J}^i = \mathbf{0}$ and ${}_O\mathbf{H}^i = \mathbf{0}$ (see [1, section 5]). The constraints guarantee the property of the body reference frame described by [1, equation (38)] and they are fulfilled automatically when using free-free modes after deleting the rigid body modes. When augmenting the free-free modes by static modes as in case of the models B7(8) and B8(9) one has two choices: one considers the constraints [1, equation (36)] when solving the multibody system equations or one renounces exploiting any properties of the Buckens-frame resulting from these constraints. In the latter case the body deformation is no longer a minimum as stated by [1, equation (38)]. In this study the second option has been used for the models B7(8) and B8(9).

In all of the models, mentioned heretofore, the modal approach has been used to describe the deformation of the beam $i = 1$ shown in Figure 3. A reference solution (*ref*) will be generated using the nodal approach. In this *reference model*, the body $i = 1$ is subdivided into 10 finite beam elements, in which a tangent-frame is used to represent the element deformation. The displacement field of the elements is interpolated in this model by linear polynomials for the longitudinal motion and by cubic ones for bending [19]. The results will be compared also with those obtained by the absolute nodal coordinate formulation (*anc*), which has been proposed recently [20]. A large reference motion of a flexible body is described by the nodal coordinates of a finite element model in this methodology [21]. The model of the beam used in this formulation has 20 elements. The displacements of the elements are interpolated by third order polynomials and the deformations are defined using a chord-frame [22].

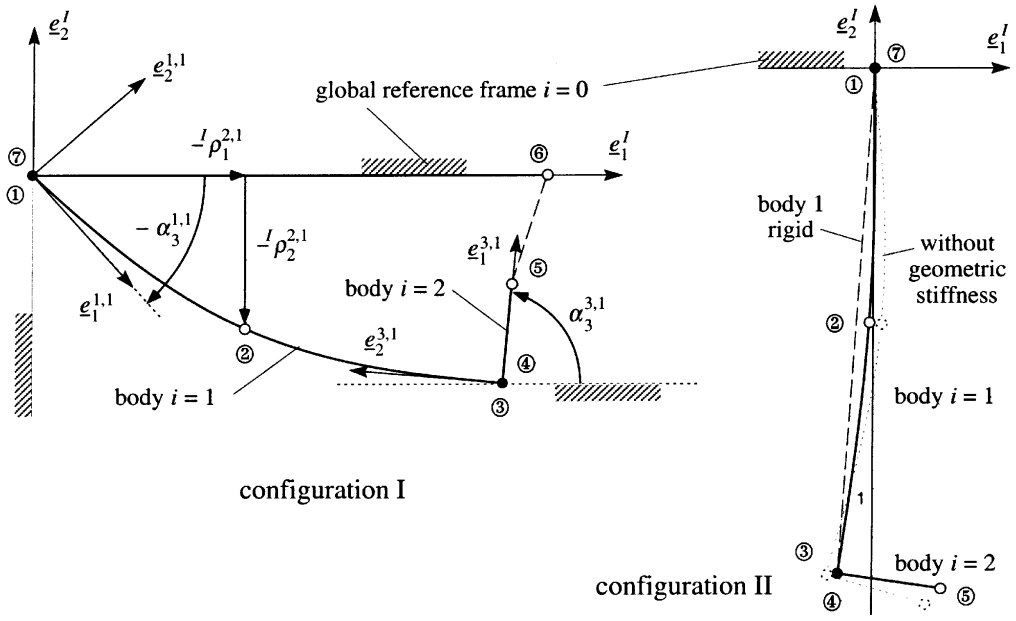

Figure 6. Equilibrium configurations I and II of the beam structure.

2.3. Deformation Results

The three problems, described at the beginning of Section 2.1, have been solved using the C1-model and both, the descriptor- and the state-space-form of the system equations. The equilibrium configurations I and II, as obtained with the Lagrangian equations of type 1, are shown in Figure 6. The motion animation of the structure found by integration of the state space equations is shown in Figure 7. In this figure, the structure configuration at selected times and the time history of the angle $\alpha_3^{3,1}$, shown in Figure 6, are depicted.

The parameters of the model have been chosen in such a way that the effect of geometric stiffening becomes important. As a consequence, the result, given in Figure 6 when neglecting those geometric stiffening terms, turns out to be wrong when compared with the solution of the reference model and with the solution, which has been obtained with a multibody code, based on the absolute nodal coordinate formulation [22]. For comparison, the equilibrium configuration II of a model, in which body $i = 1$ is rigid, is shown in Figure 6 as well.

All of the results on the motion and deformation of the structure are in a good agreement with the reference solution for all the models defined in the preceding section. This statement is detailed in Table 1. It contains results for the two equilibrium configurations I and II as obtained with various models.

The results ${}^I\rho_1^{k,i}$ and ${}^I\rho_2^{k,i}$ describe the location of the nodes $k, i = 2, 1$ and $k, i = 3, 1$ in the inertial frame and the angles $\alpha_3^{k,i}$ with $k, i = 1, 1$ and $k, i = 3, 1$ represent the orientation of $\underline{\mathbf{e}}^{k,i}$ with respect to $\underline{\mathbf{e}}^I$ (see Figure 6). For the configuration I the results are given as obtained by the models C1 and C7. Their comparison demonstrates that the complex model C7 does not significantly improve the results obtained with the simple model C1. Both of them are found to be in a good agreement with the reference solution and the results provided by the absolute nodal coordinate formulation. For the configuration II, results are presented in Table 1 as obtained with the C-, T- and B-models together with the reference results *ref* and *anc*.

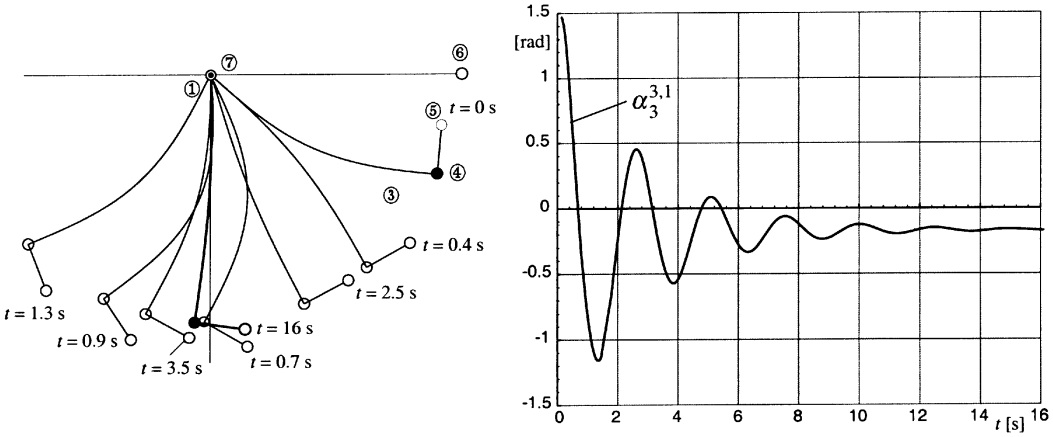

Figure 7. Motion of the beam structure from equilibrium configuration I to equilibrium configuration II.

Table 1. Results describing the deformation of body $i = 1$ in the equilibrium configurations I and II. Displacements ${}^I\rho_\alpha^{k,i}$ are given in mm and angles $\alpha_3^{k,i}$ in 10^{-3} rad.

	Configuration I		Configuration II								
Model	C1	C7	C2	C5	C7	T2	T7	B2	B7	*ref*	*anc*
${}^I\rho_1^{2,1}$	840.6	837.0	–20.5	–12.7	–19.8	–18.9	–20.0	–21.0	–19.7	–19.9	–19.8
${}^I\rho_1^{2,1}$	–5.69.8	–577.9	–1001	–1002	–1001	–1000	–1000	–1001	–1001	–1000	–999.8
${}^I\rho_1^{3,1}$	1825.5	1825.8	–137.0	–141.1	–136.1	–135.9	–136.3	–136.4	–136.1	–136.0	–136.0
${}^I\rho_2^{3,1}$	–0.817	–816.4	–1995	–1995	–1995	–1999	–1999	–1995	–1995	–1999	–1991
$\alpha_3^{1,1}$	–698.4	–721.4	–1576	–1564	–1581	–1580	–1581	–1567	–1580	–1581	–1581
$\alpha_3^{3,1}$	1427.7	1410.7	–197.5	–225.2	–237.8	–161.7	–237.1	–178.3	–237.8	–236.9	–238.3

They clearly demonstrate that all the models can be used to describe the displacements ${}^I\rho_\alpha^{k,i}$, excluding the model C5, which uses static modes only. In case of the angles $\alpha_3^{k,i}$ deviations between the results obtained with the various models are more pronounced.

In summary, the use of eigenfunctions as shape functions leads to a good representation of the system motion and of the displacements due to body deformation. Angle variables describing the deformation of the beam investigated here are still acceptable but the stresses due to body deformation, as obtained with the various models, differ significantly. This will be demonstrated now.

2.4. Stress Results

The forces and torques, required for the discussion of the internal forces due to body deformation, are defined in Figure 8. Symbols $\underline{F}^{k,i}$ and $\underline{L}^{k,i}$ denote forces and torques applied at the nodes k on body i (see [1, figure 3]). They result from force elements r and from joints s at the nodes on the bodies. Both, $\underline{F}^{k,i}$ and $\underline{L}^{k,i}$, are resolved in the bases $\underline{\mathbf{e}}^i$, shown in Figures 3 and 4 for $i = 1$ and $i = 2$, to obtain the coordinates $F_\alpha^{k,i}$ and $L_\alpha^{k,i}$. These coordinates are determined in an analysis of the multibody system using the laws for the forces and torques across the force elements and the generalized constraint forces across the joints.

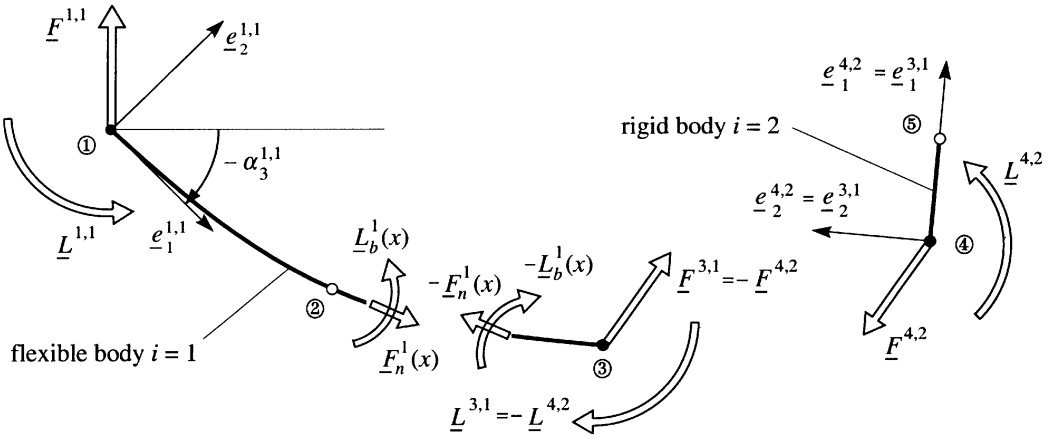

Figure 8. Interaction-forces and -torques upon the bodies of the beam structure together with internal force and moment due to deformation of the beam.

Vectors $\underline{F}_n^1(x) = F_n^1(x)\ \underline{e}_1^1$ and $\underline{L}_b^1(x) = L_b^1(x)\ \underline{e}_3^1$ represent the normal force and the bending moment applied at a cross section x of the beam. The functions $F_n^1(x)$ and $L_b^1(x)$ are found from the variables describing deformation by using the material law

$$S_{11}^1(\mathbf{R}) = \mathcal{E}^1 G_{11}^1(\mathbf{R}). \tag{3}$$

Here $S_{11}^1(\mathbf{R})$ and $G_{11}^1(\mathbf{R})$ represent stress and strain at a point $\mathbf{R}$ of the beam (see [1, figure 6]). When $x \equiv R_1$ is fixed, the stresses and strains are identical for any values of R_3 in case of the planar problem shown in Figure 3. Therefore, it is sufficient to consider $S_{11}^1(R_1, R_2) \equiv S_{11}^1(R_1, R_2, 0)$ and $G_{11}^1(R_1, R_2) \equiv G_{11}^1(R_1, R_2, 0)$. From the stress distribution $S_{11}^1(R_1, R_2)$ one obtains the normal stress S_n^1 (due to stretching) and the shear stress S_b^1 (due to bending) as

$$S_n^1(x) = S_{11}^1(x, 0) \quad \text{and} \quad S_b^1(x, R_2) = S_{11}^1(x, R_2) - S_n^1(x), \quad x \equiv R_1. \tag{4}$$

The maximum values of shear stress are obtained for $R_2 = \pm h^1/2$. The effects of the stresses $S_{11}^1(R_1, R_2)$ distributed over the rigid cross section at the point $x = R_1$ of the beam's axis can be described by a single force $\underline{F}_n^1(x)$ at $R_2 = 0$ and a moment $\underline{L}_b^1(x)$. These resultants of the system of forces acting upon the rigid cross section x are found to be

$$F_n^1(x) = A^1 S_{11}^1(x, 0) \quad \text{and} \quad L_b^1(x) = \frac{2J^1}{h^1}(S_{11}^1(x, h^1)/2) - S_n^1(x)). \tag{5}$$

The strain distribution appearing in Equation (3) is given for an Euler–Bernoulli beam by

$$G_{11}^1(R_1, R_2) = w_1'^1(x) - R_2 w_2''^1(x) + \frac{1}{2}(w_2'^1(x))^2, \quad x \equiv R_1. \tag{6}$$

The deformations w_1 and w_2 in Equation (6) are obtained from the variables $\mathbf{q}^1$, appearing in [1, equation (22)], by applying the relations given in [1, equation (43)] for $\vartheta_1 \equiv w_3 \equiv 0$. The nonlinear expression $(w_2'^1)^2$ in Equation (6) serves to develop the geometric stiffening terms due to longitudinal forces as described in [23]. The forces $F_n^1(x)$ and moments $L_b^1(x)$ are obtained using the linearized strain-displacement relations (6) in Equations (3) to (5).

The two functions $F_n^1(x)$ and $L_b^1(x)$ have to satisfy dynamical boundary conditions at $x = 0$ and $x = \ell^1$

$$F_n^1(0) = -F_1^{1,1}, \quad L_b^1(0) = -L_3^{1,1} \quad \text{and} \quad F_n^1(\ell^1) = F_1^{3,1}, \quad L_b^1(\ell^1) = L_3^{3,1}. \tag{7}$$

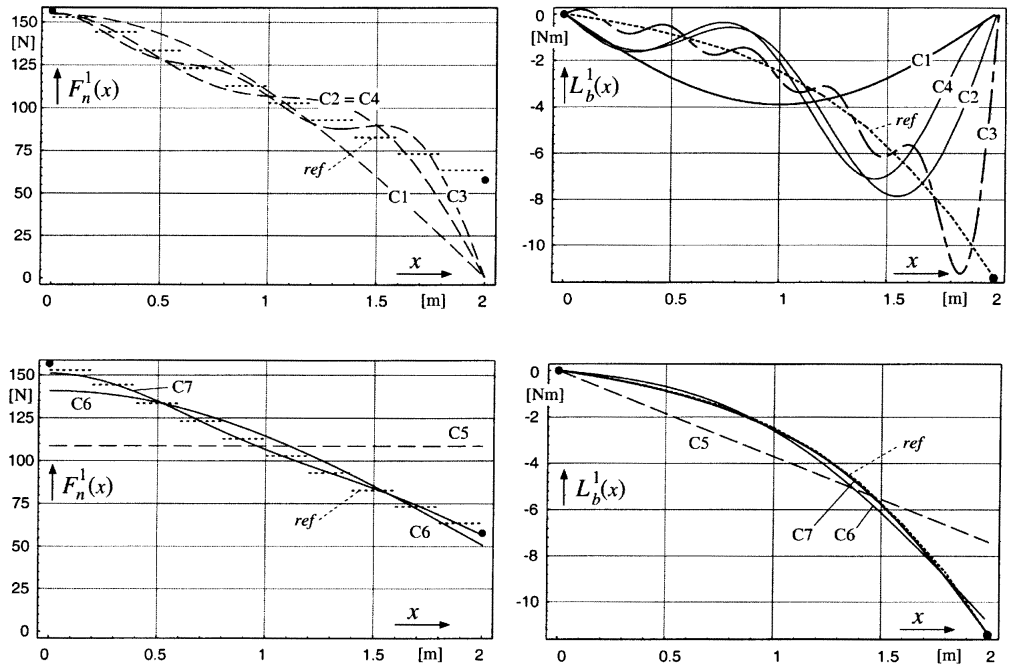

Figure 9. Normal force $F_n^1(x)$ and bending moment $L_b^1(x)$ in body 1 as obtained with the chord-frame-models for the equilibrium configuration II.

Some of the shape functions shown in Figure 5 violate these boundary conditions. In such cases the representation of stress described by the functions $F_n^1(x)$ and $L_b^1(x)$ turns out to be poor.

2.4.1. *Representation of Stress Using the Chord-Frame-Models*

A static analysis, based on the model C1, yields for the equilibrium configuration I the values

$$\left.\begin{array}{ll} F_1^{1,1} = -49.4\ \text{N}, & F_1^{3,1} = 9.0\ \text{N}, \\ L_3^{1,1} = 0\ \text{Nm}, & L_3^{3,1} = -6.9\ \text{Nm}, \end{array}\right\} \text{whereas} \left\{\begin{array}{ll} F_n^1(0) = 44.3\ \text{N}, & F_n^1(\ell^1) = 0\ \text{N}, \\ L_b^1(0) = 0\ \text{Nm}, & L_b^1(\ell^1) = 0\ \text{Nm}. \end{array}\right. \tag{8}$$

It is obvious that the shape functions used in the C1-model cannot satisfy the dynamical boundary conditions of Equation (7). A similar result is obtained by an analysis of the equilibrium configuration II. In this case, the model C1 results in

$$\left.\begin{array}{ll} F_1^{1,1} = -157.4\ \text{N}, & F_1^{3,1} = 58.7\ \text{N}, \\ L_3^{1,1} = 0\ \text{Nm}, & L_3^{3,1} = -11.6\ \text{Nm}, \end{array}\right\} \text{whereas} \left\{\begin{array}{ll} F_n^1(0) = 145.7\ \text{N}, & F_n^1(\ell^1) = 0\ \text{N}, \\ L_b^1(0) = 0\ \text{Nm}, & L_b^1(\ell^1) = 0\ \text{Nm}. \end{array}\right. \tag{9}$$

Because of the violation of the dynamical boundary conditions, the representation of the internal forces $F_n^1(x)$ and moments $L_b^1(x)$ is not satisfactory. Such behaviour, i.e. good motion and deformation results and poor stresses, suggests that one may determine the deformations by multibody simulation programs and compute the stresses, using post-processor finite element codes [2, 12]. However, an acceptable representation of stresses can also be obtained with multibody models using quasi-comparison functions. This will be demonstrated now, considering all of the chord-frame models introduced above.

Figure 9 shows the functions $F_n^1(x)$ and $L_b^1(x)$ for the equilibrium configuration II, when using the chord-frame models. The reference solution obtained with the finite element method

is denoted by *ref* in the diagrams. In the reference model the displacement field of the finite elements is interpolated by linear polynomials for the longitudinal motion. This explains, why the element normal forces are constant, resulting in the discontinuities of the reference solution for $F_n^1(x)$ in Figure 9. The points (•), marked in the diagrams at $x = 0$ and $x = \ell^1$, represent the values of the forces $F_1^{k,i}$ and the torques $L_3^{k,i}$ at the nodes $k = 1$ and $k = 3$, as obtained with the reference solution from the constraint forces in the joints. These results are

$$F_1^{1,1} = -157.7 \text{ N}, \quad L_3^{1,1} = 0 \text{ Nm}, \quad F_1^{3,1} = 58.8 \text{ N}, \quad L_3^{3,1} = -11.44 \text{ Nm}. \tag{10}$$

The internal forces at the boundaries $x = 0$ and $x = \ell^1$ found with the reference solution have slightly different values. They are, together with the force F_n^1 and the moment L_b^1 at the node $k = 2$ on body $i = 1$

$$\begin{aligned} F_n^1(0) &= 152.8 \text{ N}, \quad F_n^1(\ell^1/2) = 108.3 \text{ N}, \quad F_n^1(\ell^1) = 63.8 \text{ N}, \\ L_b^1(0) &= 0 \text{ Nm}, \quad L_b^1(\ell^1/2) = -2.47 \text{ Nm}, \quad L_b^1(\ell^1) = -11.37 \text{ Nm}. \end{aligned} \tag{11}$$

The results presented in Figure 9 demonstrate that the eigenfunctions used in the models C1 to C3 cannot satisfy the dynamical boundary conditions. The functions minimize a mean value of the errors, as suggested by the Ritz method. By adding more functions, the error becomes smaller, but as demonstrated clearly by the results of the C3-model for $L_b^1(x)$, the solution starts to oscillate heavily in the neighbourhood of $x = \ell^1$ when using higher numbers of eigenfunctions, which are unable to satisfy the dynamical boundary condition $L_b^1(\ell^1) = L_3^{3,1}$. Such a behaviour is similar to Gibb's phenomenon, as known from the representation of discontinuous functions by Fourier series, e.g. [24, p. 392]. Selecting the transformed eigenfunctions of a beam supported by a rotational joint at $x = 0$ does not improve the solution, as demonstrated by the results obtained with the C4-model. The results of the model C5 demonstrate that the static deformation modes yield nonzero values for all of the forces and moments, which had been enforced by the eigenfunctions to disappear. The representation of $F_n^1(x)$ and $L_b^1(x)$ by the static modes only is poor. But combining their capability to satisfy the dynamical boundary conditions with the ability of the eigenfunctions to represent $F_n^1(x)$ and $L_b^1(x)$, convergence is significantly improved, as demonstrated by the results of the C6- and C7-models.

2.4.2. *Representation of Stress Using the Tangent-Frame-Models*
Figure 10 shows the results, when using a tangent-frame (the T-models, defined previously). Eigenfunctions and static deformation modes for the longitudinal motion are identical for chord- and tangent-frames, which implies that the force representations, obtained by the C- and T-models, do not differ. This explains why Figure 10 shows $L_b^1(x)$ only. The chord-frame results to be compared with the tangent-frame results are shown in Figure 10 again. The T-models yield larger errors than the corresponding C-models. The errors result from violation of the dynamical boundary condition at $x = 0$, which is enforced by the eigenfunctions satisfying the chord-frame conditions (see diagrams for T2 and C2). As in case of the C-models, the representation of $L_b^1(x)$ is improved, when adding static modes, but the errors of the T-models remain larger than those obtained with the corresponding C-models.

2.4.3. *Representation of Stress Using the Buckens-Frame-Models*
Finally, Figure 11 shows the functions $F_n^1(x)$ and $L_b^1(x)$ when using a Buckens-frame defined by the linearized equations (36) from [1]. These conditions are satisfied automatically, when using eigenfunctions of a free-free beam after deleting the rigid body modes. By contrast

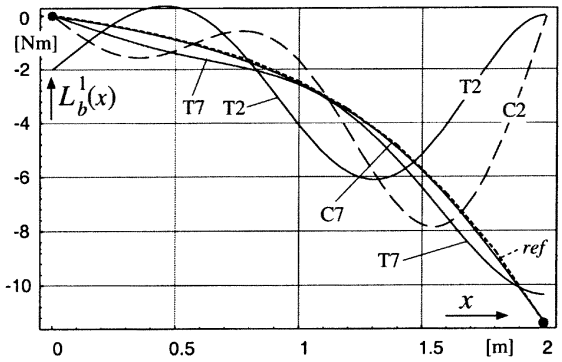

Figure 10. Normal force $F_n^1(x)$ and bending moment $L_b^1(x)$ in body 1 as obtained with the tangent-frame-models. For comparison, the results determined with the corresponding C-models are presented, too.

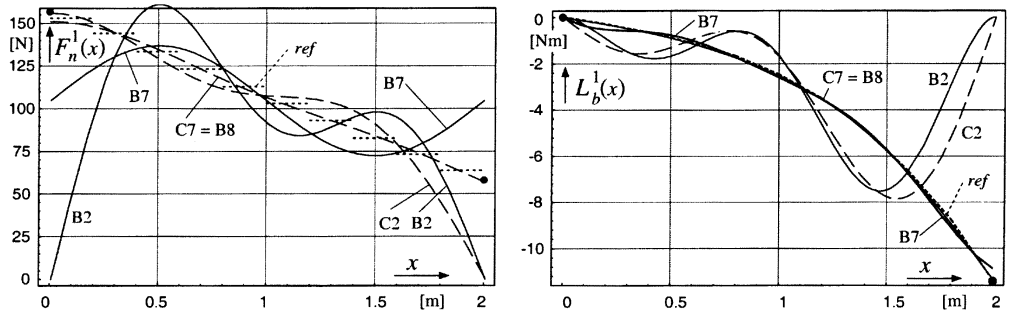

Figure 11. Normal force $F_n^1(x)$ and bending moment $L_b^1(x)$ in body 1 as obtained with the Buckens- or mean-axes-frame-models together with the results provided by the corresponding C-models.

with the eigenfunctions of a simply supported beam, satisfying $F_n^1(0) \neq 0$, those of a free-free beam yield $F_n^1(0) = 0$. As a consequence, the errors in the representation of $F_n^1(x)$ are increased in the model B2 as compared to C2. When adding the static modes used in the C5-model to obtain the B7-model, the representation of the moment $L_b^1(x)$ is improved, providing an approximation similar to the one obtained by the model C7. But the representation of the force $F_n^1(x)$ with the B7-model is still insufficient as compared to the C7-model. The reason is simple: by adding the static mode for longitudinal deformation of the C5-model to the eigenfunctions of the free-free beam, one has the freedom to represent nonzero forces at $x = 0$ and $x = \ell^1$, but these have to be identical (see diagram B7 for $F_n^1(x)$. Only after adding another static mode to obtain the B8-model, different forces at $x = 0$ and $x = \ell^1$ can be represented by the system of static forms and eigenfunctions. As a consequence, the B8-model yields an approximation of $F_n^1(x)$ of roughly the same accuracy as C7. The plots for the two models C7 and B8 cannot be distinguished in a diagram as shown in Figure 11.

2.5. Concluding Remarks

An analysis of the problem shown in Figure 1 verifies the statements given in [1, section 1] on body deformation: the results demonstrate that admissible functions (here eigenfunctions of various types) yield an acceptable representation of body deformation, as suggested by the expansion theorem detailed in [25, vol I, p. 311] or [26, p. 111]. When the admissible

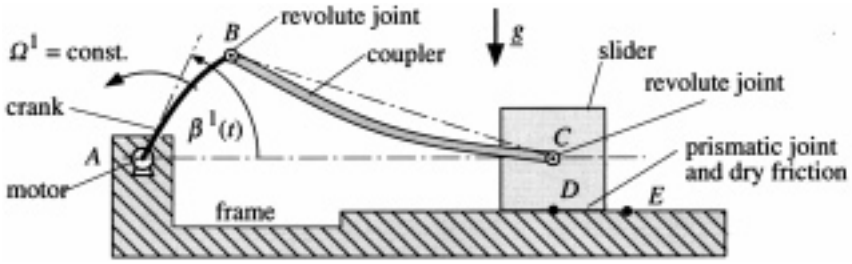

Figure 12. Slider/crank mechanism with elastic elements.

functions violate the dynamical boundary conditions, an acceptable representation of the stresses is obtained by high numbers of shape functions only. In particular, at points where the admissible functions violate the dynamical boundary conditions a behavior similar to Gibb's phenomenon is observed. Quasi-comparison functions (here a combination of eigenmodes and static modes) result in a significant improvement of the representation of stress.

3. Range of Validity of Linearized Equations

A second example, the slider/crank mechanism shown in Figure 12, is used to demonstrate the influence of the choice of the body reference frame on the range of validity of the linearized equations of motion [1, equation (26)]. It is studied by analysing

- the equilibrium configurations I and II of the mechanism, obtained when fixing the angle β^1 to the values $\beta^1 = 0°$ and $\beta^1 = 57.3°$, respectively;
- its motion due to a driving torque, sustaining a constant angular velocity Ω^1.

To define problems with unique solutions, the friction force in the prismatic joint at D is assumed to be zero for the determination of the equilibrium configurations.

3.1. Description of the Models

The multibody model of the mechanism is shown in Figure 13. The models of crank and coupler are Euler–Bernoulli beams and the slider is assumed to be rigid. The data of bodies $i = 1$ and 2 are with reference to the labelling scheme shown in Figure 13 and using notation by analogy with the previous example: $\ell^1 = 0.6$ m, $\ell^2 = 2.0$ m, $A^i = 0.0006$ m^2, $J^i = 4.5 \cdot 10^{-10}$ m^4, $\rho^i = 8400$ kg/m^3 and $\mathcal{E}^i = 7 \cdot 10^{10}$ Nm^2. The data of body 3 are: $m^3 = 8.4$ kg, $I^3 = 0.028$ kg m^2, where I^3 is given with respect to O^3. The latter point coincides with the center of mass CM^3. The axes of the joints are clear from the figures, and the dry friction coefficient in the prismatic joint (force element $r = 5$) is $\nu = 0.05$. The driving angular velocity is $\Omega^1 = 0.2$ rad/s and the gravitational acceleration in the inertial frame is $[0, -g, 0]^T$, $g = 9.81$ m/s^2.

The descriptor form of system representation has been used to solve the problems formulated above. In this form the system motion is described by $\mathbf{z}_I = [\mathbf{z}_I^i]$ and $\mathbf{z}_{II} = [\mathbf{z}_{II}^i]$, with $\mathbf{z}_I^i$ and $\mathbf{z}_{II}^i$ defined in [1, equation (22)], and by the Lagrangian multipliers $\boldsymbol{\mu}$ representing the constraint forces across the joints. In a preliminary analysis the deformation w_2^1 of the crank, as given by Equation (2), is described using the tangent-frame shown in Figure 13 and the first eigenmode of a cantilever beam. The deformation w_2^2 of the coupler is represented using a chord-frame and the first mode of a simply supported beam. Longitudinal deformations

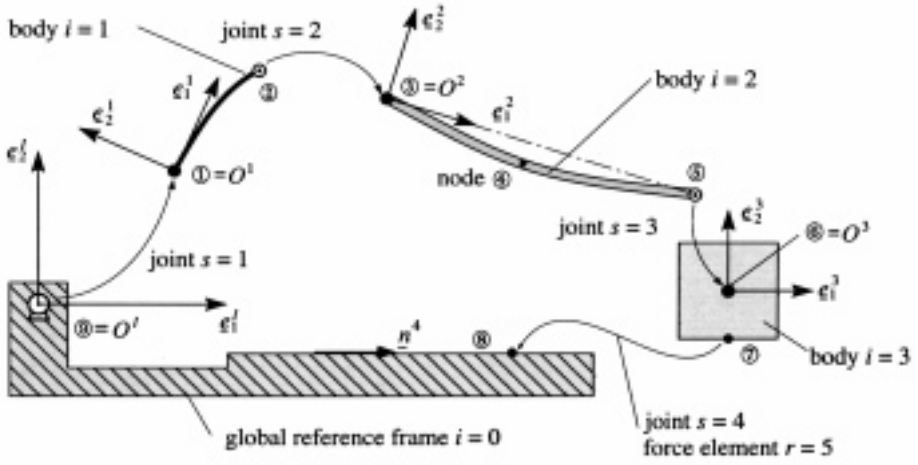

Figure 13. Multibody model of the slider/crank mechanism. Node $k, i = 8, 0$ is at E from Figure 12, where $D = E$ when $\beta^1 = 0°$ and when the bodies are not deformed. Vector $\underline{n}^4$ represents the axis of joint $s = 4$.

Table 2. Models used to study the effects of substructuring and definition of body reference frame.

model	crank, body $i = 1$	coupler, body $i = 2$
A	*one* body, *tangent-frame, one* bending mode of a cantilever beam.	*one* body, *chord-frame, one* bending mode of a simply supported beam.
B	as in model A.	*two* bodies, *chord-frame* and *one* bending mode of a simply supported beam each.
C	as in model A.	*two* bodies, *tangent-frames* and *one* bending mode of a cantilever beam each.
D	*one* body, *chord-frame* and *one* bending mode of a simply supported beam.	as in model B.
ref	*two* bodies, *chord-frame* and *one* bending mode of a simply supported beam each, together with *two* static modes, due to a force F^2 and a torque L^3 at $x = \ell^1/2$.	*three* bodies, *chord-frame* and *one* bending mode of a simply supported beam each, together with *two* static modes, due to torques L^3 at $x = 0$ and $x = \ell^2/3$.
anc	absolute nodal coordinate formulation using 8 elements – deformation of the elements is described using a chord-frame. The linearized strain-displacement relations (6) are used.	as for body $i = 1$ but 20 elements.

$w_1^i, i = 1, 2$ are neglected for both of the bodies. This model is denoted as model A in Table 2. The remainder of models to be used later are described in the table in a similar way.

3.2. Results Obtained Using Model A

The equilibrium configurations I and II and the motion of the mechanism for one revolution of the crank, as obtained by the model A, are shown in Figures 14 and 15.

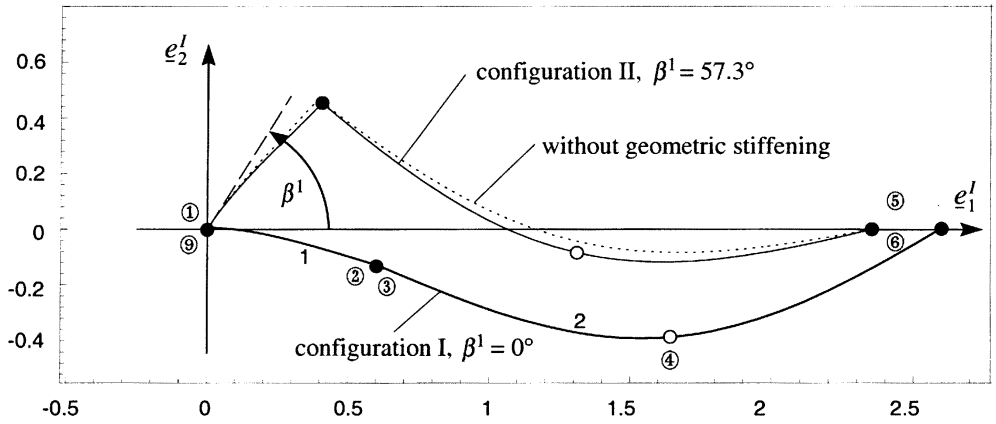

Figure 14. Equilibrium configurations I and II of the mechanism as obtained by model A.

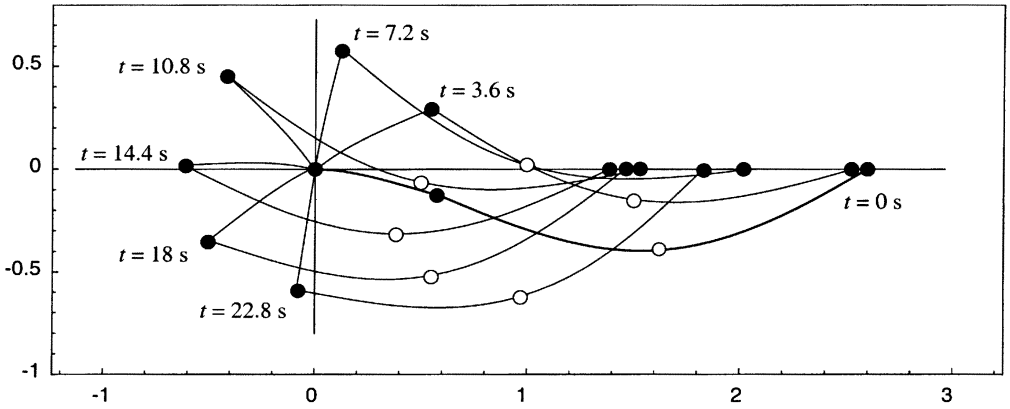

Figure 15. Configurations of the mechanism during motion for times $0 \leq t \leq 22.8$ s as obtained by model A.

The motion has been determined by solving the Lagrangian equations of type 1, applying the DAE-solver ODASSL described in [27]. An equilibrium configuration II, obtained without considering geometric stiffening, is shown in Figure 14 as well. The shape functions used here do not satisfy the dynamical boundary conditions and as a consequence the representation of internal forces turns out to be poor. Details can be found in [28].

The results shown in Figures 14 and 15 demonstrate that the deformations, especially those of the coupler, are quite large. In case of the equilibrium configuration I ($\beta^1 = 0°$), one observes that the rotational displacement of the beam cross section at the node $k, i = 5, 2$ becomes $\vartheta_3^{5,2} = 0.51$ rad = 29.5°. This is far beyond the values acceptable for an application of the Equations (26) from [1], when linearized assuming the deformations to be small (see also [1, equations (16) and (20)]).

3.3. Models Reducing the Magnitude of Deformation

The magnitude of the deformations may be reduced, considering two possibilities to improve modelling: one may subdivide the flexible bodies, as proposed in [17], and one may modify the body reference frame to minimize the magnitude of deformations [1, figure 5]. Various options will be analyzed now for the case of the equilibrium configuration I, using the models

Table 3. Values characterising the equilibrium configuration I as obtained with the models defined in Table 2.

model	A	B	C	D	*ref*	*anc*
location ${}^I\rho_2^{2,1}$ of node 2,1 in $\{O^I, \underline{\mathbf{e}}^I\}$ [m]	–0.134	–0.134	–0.136	–0.079	–0.132	–0.130
location ${}^I\rho_2^{4,2}$ of node 4,2 in $\{O^I, \underline{\mathbf{e}}^I\}$ [m]	–0.394	–0.277	–0.253	–0.250	–0.359	–0.355
location ${}^I\rho_1^{6,3}$ of node 6,3 in $\{O^I, \underline{\mathbf{e}}^I\}$ [m]	2.596	2.551	2.621	2.548	2.481	2.470
angle $\alpha_3^{2,1}$ at node 2,1 [rad]	–0.307	–0.308	–0.312	–0.264	–0.326	–0.322
angle $\alpha_3^{3,2}$ at node 3,2 [rad]	–0.447	–0.356	–0.265	–0.385	–0.412	–0.409
angle $\alpha_3^{4,2}$ at node 4,2 [rad]	0.067	0.071	0.059	0.042	0.072	0.071
angle $\alpha_3^{5,2}$ at node 5,2 [rad]	0.581	0.490	0.371	0.463	0.547	0.542
deformation $\vartheta_3^{2,1}$ at node 2,1 [rad]	–0.307	–0.308	–0.312	–0.132	–0.074	–0.0014
deformation $\vartheta_3^{3,2}$ at node 3,2 [rad]	–0.514	–0.214	0.0	–0.213	–0.090	–0.0023
deformation $\vartheta_3^{5,2}$ at node 5,2 [rad]	0.514	0.209	0.430	0.211	0.088	–0.0023
bending torque $L_b^{1,1} = -\mu_3$ at node 1,1 [Nm]	–38.1	–38.3	–38.7	–38.1	–37.4	–37.18
bending torque $L_b^{4,2}$ at node 4,2 [Nm]	25.4	0.0	34.6	0.0	22.9	22.76

described in Table 2. Only chord- and tangent-frames are considered, because the orientation of a Buckens-frame is not modified as compared to a chord-frame in case of the beam models used here – for a discussion of the orientation of a Buckens-frame see also [29]. Moreover, a shift of the origin of the body reference frame to the center of mass, resulting from a choice of a Buckens-frame, does not affect the magnitude of the angles leading to the problem mentioned above.

In case of model B, the coupler is subdivided into two bodies, interconnected by a bracket joint. Deformations of the subbodies are represented by the first eigenmode of a simply supported beam, as suggested by the boundary conditions of a chord-frame. In model C this chord-frame is replaced by a tangent-frame, using the first eigenmode of a cantilever beam. In case of D the coupler is modelled as in B and to reduce the magnitude of deformations of the crank, a chord-frame is used instead of the tangent-frame.

The models A to D allow an analysis of the size of deformations due to substructuring and to the choice of body reference frames. The corresponding results for the equilibrium configuration I are given in Figure 16 and Table 3. Deformations of the coupler are significantly smaller when using model B instead of A: angle $\vartheta_3^{5,2}$ is reduced from 0.514 rad to 0.209 rad. Model C demonstrates that this is true only when using a chord-frame. The choice of a tangent-frame does not pay off, when trying to reduce the magnitude of deformation, a fact, which is suggested also by [1, figure 5]. Angle $\vartheta_3^{5,2}$ is reduced by subdividing the coupler but, as demonstrated by the values of $\vartheta_3^{2,1}$ for A, B and C in Table 3, the deformation

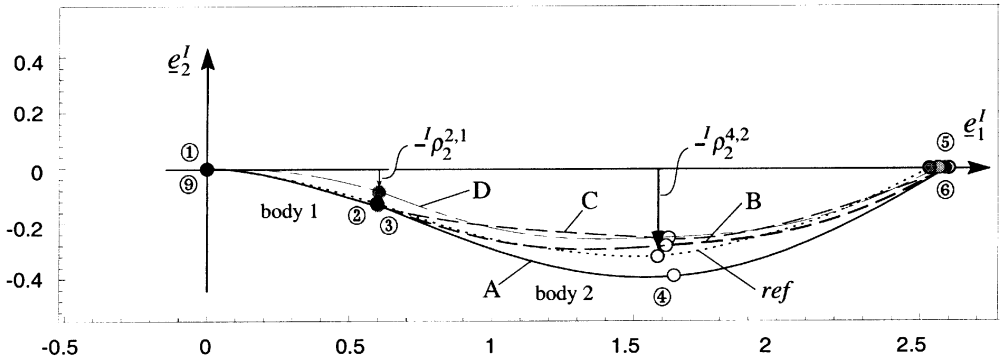

Figure 16. Equilibrium configurations I of slider/crank mechanism as obtained by the models A to D and *ref*. Models A and C result in deformations too large for application of linearized equations.

of the crank is still too large. It is reduced in model D by selecting a chord-frame and the corresponding eigenmode. This yields a value of $\vartheta_3^{2,1} = -0.132$ rad. If this is still considered too large for linearization, the bodies may be subdivided further, as suggested for the *ref*-model defined in Table 2.

The analysis demonstrates that the deformations may be kept small enough as to justify an application of the linearized equations [1, equation (26)]. The goal may be achieved by subdividing the bodies and using chord-frames. But the previous example demonstrates that one cannot expect to represent body deformations, and especially internal forces, properly, when using one mode only. Sources of the deficiencies of the models A to D may be found by looking at the values of Table 3: whereas models A to C yield coordinates ${}^I\rho_2^{2,1}$ of vector $\underline{\rho}^{2,1}$ in the inertial frame, i.e. of the location of node $k, i = 2, 1$, of ca. -0.13 m, the same value is lowered to -0.079 m in model D. The problems become even more apparent when comparing with the solution *anc*, obtained with a finite element model based on the absolute nodal coordinate formulation as described in the last row of Table 2. The results found with this model (last column of Table 3) can be approximated closely by the *ref*-model from Table 2. In this case static modes are used to satisfy the dynamical boundary conditions. The resulting equilibrium configuration I is marked in Figure 16 by *ref*. The plot cannot be distinguished from the one obtained with the *anc*-model. Based on the results of this analysis of the equilibrium configuration I, one can recompute the equilibrium configuration II and the system motion, using the *ref*-model to obtain more reliable results. Because of the preliminary analysis, these computations can be done with an efficient model based on the modal approach. For the analysis of the mechanism motion one may want to add static modes to satisfy dynamical boundary conditions due to the driving torque.

All of the results have been obtained using Mathematica, Version 2.2. The corresponding notebook files may be found at http://www.vieweg.de/downloads.

4. Conclusions

The floating frame of reference formulation is based on a separation of the flexible body motion into a reference motion and a deformation. The definition of the two motions requires the specification of a body reference frame, which in turn is tied to the choice of shape functions

in the Ritz method. Two statements have been verified by discussion of the derivation of the system equations in [1] and the examples considered here:

1. The modal approach to represent body deformation may reduce the number of system variables considerably and thus increases computational efficiency, but it raises the problem of how to select the shape functions. Quasi-comparison functions, obtained by combining eigenfunctions (satisfying equations resulting from the definition of the body reference frame) with static modes to satisfy the dynamical boundary conditions, significantly improve the representation of internal forces, i.e. stresses. This statement applies for any choice of the body frame and the corresponding shape functions, but specific choices may require less variables than others. The effort required for selection of the suitable quasi-comparison functions pays off: in addition to an increased efficiency of multibody simulation, it often eliminates the need for finite element post-processing the simulation results to obtain the stresses.
2. The linearization of the system equations requires the deformations to be as small as possible. This is guaranteed by selecting a so-called Buckens-frame as a body reference frame. If the orientation of the Buckens-frame is not significantly affected by deformation, a properly chosen chord-frame serves the purpose as well. In addition, deformations can be kept small by subdividing flexible bodies. A preliminary analysis of simple problems may provide the numbers of subbodies and shape functions required for the representation of deformation and internal forces in more complicated problems. Efficient models, found by following such routes, increase the efficiency of multibody system analysis.

In summary, the results improve the computational efficiency of multibody codes and they increase the range of validity of the linearized system equations, often used in the floating frame of reference approach.

References

1. Schwertassek, R., Wallrapp, O., and Shabana, A. A., 'Flexible multibody simulation and choice of shape functions', *Nonlinear Dynamics*, to appear.
2. Dietz, S., Netter, H., and Sachau, D., 'Fatigue life prediction by coupling FEM and MBS calculations', Paper presented at the First Symposium on Multibody Dynamics and Vibration at 16th Annual ASME Conference on Mechanical Vibration and Noise, Sacramento, CA, 1997.
3. Meirovitch, L. and Kwak, M. K., 'Convergence of the classical Rayleigh–Ritz method and the finite element method', *AIAA Journal* **28**(8), 1990, 1509–1516.
4. Meirovitch, L. and Kwak, M. K., 'On the modeling of flexible multi-body systems by the Rayleigh–Ritz method', Paper presented at the AIAA Dynamics Specialists Conference, Long Beach, CA, April, 1990.
5. Meirovitch, L. and Hagedorn, P., 'A new approach to the modelling of distributed non-self-adjoined systems', *Journal of Sound and Vibration* **178**(2), 1994, 227–241.
6. Hagedorn, P., 'Quasi-comparison functions in the dynamics of elastic multibody systems', in *Dynamics and Control of Large Structures, Proceedings of the 8th VPI&SU Symposium*, Blacksburg, VA, May 6–8, L. Meirovitch (ed.), 1991, pp. 97–108.
7. Hagedorn, P., 'The Rayleigh–Ritz method with quasi-comparison functions in nonself-adjoint problems', *Journal of Vibration and Acoustics* **115**, 1993, 280–284.
8. Géradin, M., Cardona, A., Doan, D. B., and Duysens, J., 'Finite element modelling concepts in multibody dynamics', in *Computer Aided Analysis of Rigid and Flexible Mechanical Systems*, M. F. Pereira and J. Ambrosio (eds.), Kluwer Academic Publishers, Dordrecht, 1994, pp. 233–284.
9. Hänle, U., 'Modellierung und Berechnung dynamisch beanspruchter elastischer Strukturen bei endlichen Rotationen', Dissertation, Universität Stuttgart, 1995.

10. Marthinsen, A. and Sivertsen, O. I., 'Parallelization of large mechanical engineering codes', in *Computational Methods in Mechanical Systems*, J. Angeles and E. Zakhariev (eds.), Springer-Verlag, Berlin, 1997, pp. 364–381.
11. Popp, K., Dirr, B., and Jahnke, M., 'Analysis of flexible parts in multibody systems using finite element methods', in *Dynamics and Control of Large Structures, Proceedings of the 8th VPI&SU Symposium*, Blacksburg, VA, May 6–8, L. Meirovitch (ed.), 1991, pp. 393–404.
12. Jahnke, M., *Ein Beitrag zur Untersuchung elastischer Mehrkörpersysteme unter Nutzung von Finite-Elemente-Software*, Fortschritt-Bericht VDI, Reihe 11: Schwingungstechnik, Nr. 214, VDI-Verlag, Düsseldorf, 1994.
13. Ambrosio, J. A. C. and Pereira, M. F. S., 'Flexible multibody dynamics with nonlinear deformations: Vehicle dynamics and crashworthiness applications', in *Computational Methods in Mechanical Systems*, J. Angeles and E. Zakhariev (eds.), Springer-Verlag, Berlin, 1997, pp. 382–419.
14. Yim, H. J., Dopker, B., and Haug, E. J., 'Computational methods for stress analysis of mechanical components in dynamic systems', Paper presented at the 1st Annual Symposium on Mechanical System Design in a Concurrent Engineering Environment, Iowa City, IA, 1989.
15. Ryu, J., Sung-Sup-Kim, and Sang-Soo-Kim, 'An efficient computational method for dynamic stress analysis of flexible multibody systems', *Computers & Structures* **42**(6), 1992, 969–977.
16. Melzer, F., 'Symbolisch-numerische Modellierung elastischer Mehrkörpersysteme mit Anwendung auf rechnerische Lebensdauervorhersagen', Dissertation, Universität Stuttgart, 1993.
17. Wu, S. C. and Haug, E. J., 'Geometric nonlinear substructuring for dynamics of flexible mechanical systems', *International Journal of Numerical Methods in Engineering* **26**, 1988, 2211–2226.
18. Shabana, A. A., 'Resonance conditions and deformable body coordinate systems', *Journal of Sound and Vibration* **192**(1), 1996, 389–398.
19. Zienkiewicz, O. C. and Taylor, R. L., *The Finite Element Method: Solid and Fluid Mechanics Dynamics and Non-linearity*, Vol. 2, McGraw-Hill, London, 1991.
20. Shabana, A. A., 'An absolute nodal coordinate formulation for the large rotation and deformation analysis of flexible bodies', Report, Mechanical Engineering, University of Illinois at Chicago, 1996.
21. Shabana, A. A. and Schwertassek, R., 'Equivalence of the floating frame of reference approach and finite element formulations', *International Journal of Non-Linear Mechanics* **33**(3), 1998, 417–432.
22. von Dombrowski, S. and Schwertassek, R., 'Analysis of large flexible body deformation using absolute coordinates', Paper presented at the Euromech Colloquium 404, Advances in Computational Multibody Dynamics, Lisboa, Portugal, 1999.
23. Schwertassek, R., 'Flexible bodies in multibody systems', in *Computational Methods in Mechanical Systems*, J. Angeles and E. Zakhariev (eds.), Springer-Verlag, Berlin, 1997, pp. 329–363.
24. Knopp, K., *Theorie und Anwendung der unendlichen Reihen*, Springer-Verlag, Berlin, 1947.
25. Courant, R. and Hilbert, D., *Methoden der mathematischen Physik*, Springer-Verlag, Berlin, 1968.
26. Tychonoff, A. N. and Samarski, A. A., *Differentialgleichungen der mathematischen Physik*, Deutscher Verlag der Wissenschaften, Berlin, 1959.
27. Eich-Soellner, E. and Führer C., *Numerical Methods in Multibody Dynamics*, Teubner, Stuttgart, 1998.
28. Schwertassek, R. and Wallrapp, O., *Dynamik flexibler Mehrkörpersysteme*, Vieweg, Braunschweig, 1999.
29. Milne, R. D., 'Some remarks on the dynamics of deformable bodies', *AIAA Journal* **6**(3), 1968, 556–558.